• Human Brain Mapping 3:190–208(1995) •

Automatic 3-D Model-Based Neuroanatomical Segmentation

D.L. Collins, C.J. Holmes, T.M. Peters, and A.C. Evans

McConnell Brain Imaging Centre, Montreal Neurological Institute, McGill University, Montreal, Canada

Abstract: Explicit segmentation is required for many forms of quantitative neuroanatomic analysis. However, manual methods are time-consuming and subject to errors in both accuracy and reproducibility (precision). A 3-D model-based segmentation method is presented in this paper for the completely automatic identification and delineation of gross anatomical structures of the human brain based on their appearance in magnetic resonance images (MRI).

The approach depends on a general, iterative, hierarchical non-linear registration procedure and a 3-D digital model of human brain anatomy that contains both volumetric intensity-based data and a geometric atlas. Here, the traditional segmentation strategy is inverted: instead of matching geometric contours from an idealized atlas directly to the MRI data, segmentation is achieved by identifying the non-linear spatial transformation that best maps corresponding intensity-based features between a model image and a new MRI brain volume. When completed, atlas contours defined on the model image are mapped through the same transformation to segment and label individual structures in the new data set.

Using manually segmented structure boundaries for comparison, measures of volumetric difference and volumetric overlap were less than 2% and better than 97% for realistic brain phantom data, and less than 10% and better than 85%, respectively, for human MRI data. This compares favorably to intra-observer variability estimates of 4.9% and 87%, respectively. The procedure performs well, is objective and its implementation robust. The procedure requires no manual intervention, and is thus applicable to studies of large numbers of subjects. The general method for non-linear image matching is also useful for non-linear mapping of brain data sets into stereotaxic space if the target volume is already in stereotaxic space. © 1995 Wiley-Liss, Inc.

Key words: model-based segmentation, non-linear deformation, MRI, human brain

INTRODUCTION

The ability to easily modify scanning parameters, and thus control image contrast between different structures of interest, has made magnetic resonance imaging (MRI) the modality of choice for neuroanatomical studies. The three-dimensional (3-D) nature of the data permits detailed in vivo examination of different structures and their spatial inter-relationships. While qualitative analysis may be sufficient for disease diagnosis, quantitative analysis of specific regions is required for longitudinal monitoring of disease progression or remission [Arnold et al., 1992], pre-operative evaluation and surgical planning [Kelly et al., 1983; Kall et al., 1987; Peters et al., 1990], radiosurgery and radiotherapy treatment planning

Received for publication April 21, 1995; revision accepted August 21, 1995.

Address reprint requests to D. Louis Collins, c/o Dr. Alan Evans, Montreal Neurological Institute, WB 320, 3801 University St., Montreal, Quebec, Canada H3A 2B4.

© 1996 Wiley-Liss, Inc.

[Schade et al., 1987; Sontag et al., 1986], mapping of functional neuroanatomy of sensorimotor and cognitive processes [Fox et al., 1985; Evans et al., 1992b; Bohm et al., 1992] as well as the analysis of neuroanatomical variability among normal brains [Evans et al., 1992a, 1993, 1994; Sorlie et al., 1995].

Quantitative regional analysis is possible only with explicit segmentation[1] to separate and identify structures. This is often achieved using a brain atlas as a guide for anatomical localization and functional interpretation (e.g., Talairaich and Tournoux, 1988; Bohm et al., 1991; Seitz et al., 1990; Evans et al., 1991b; Bajcsy and Kovacic, 1989), where it is assumed that there exists a topographical invariance among normal subjects. Manual segmentation is achieved by determining the spatial transformation required to map the atlas data to the brain image volume for a given individual. Hence, segmentation becomes a registration problem: features from the atlas (e.g., landmark points, edges and regions of similar intensity) must be registered with corresponding features from the tomographic data in order to determine the contours for a particular structure.

While certainly more reliable than free-hand contouring, manually directed atlas customization is still tedious, difficult and time consuming. Errors occur because of subjectivity in atlas slice selection, structure interpretation, poor software interface design, poor eye-hand coordination, low tissue contrast, image degradation caused by artefacts and noise, and edge blurring due to partial volume effects (tissue mixing within a single voxel) and, perhaps most importantly, to the fact that tomographic slices are often not scanned at the same orientation as the atlas. We present here a fully automated 3-D non-linear matching algorithm which overcomes these difficulties to achieve a robust, objective regional segmentation of normal anatomy.

The non-linear algorithm, denoted ANIMAL (*A*utomated *N*onlinear *I*mage *M*atching and *A*natomical *L*abelling), has been presented before in the context of spatial normalization of image volumes to stereotaxic space [Collins et al., 1994b]. It is an extension of a previously reported linear method for stereotaxic normalization [Collins et al., 1994a]. In this paper we concentrate on the use of this non-linear procedure for automatic labelling of brain structures according to some predefined segmentation scheme. The two perspectives are combined within the concept of probabilistic neuroanatomical atlases. In this approach, large ensembles of brain data are first labelled in their native space and then mapped into some stereotaxic space with a limited number of degrees of freedom, e.g., 9- or 12-parameter affine transform. The likelihood of any structure label occurring at any stereotaxic voxel gives rise to a probability function for each structure which, when expressed for all structures, gives rise to a probabilistic anatomical atlas.

Previous work

Most classification techniques applied to the segmentation problem can identify gross tissue types such as cerebro-spinal fluid and white or grey matter (see [Bezdek et al., 1993] for a good review). However, these methods cannot identify individual neuroanatomical structures. While computer vision-based or image processing-based algorithms delineate elementary regions from the image data based on measures of local intensity properties through scale space (e.g., [Pizer et al., 1990]), these regions are not anatomically labelled nor do their borders always correspond to the outline of a cerebral structure. External domain-specific information must be used to interpret the features present in an image.

Segmentation is distinct from classification in that the goal is to identify specific structures. Any fully automatic regional segmentation method must employ some form of model-based information to constrain the problem. Techniques from artificial intelligence such as expert systems represent this information in the form of semantic rules to manipulate previously extracted features [Vernazza et al., 1987; Arata et al., 1991; Dhawan and Arata, 1992]. Some of these methods become complex and unwieldy when dealing with many structures and most are highly sensitive to the nature of a pre-segmentation step required to extract the features.

Merging classification techniques with linear registration methods, Zachmann [1991] has matched a given data set to an iconic model (a voxelated volume, where the value in each voxel represents the probability of existence of a structure) for classification of the fluid spaces of the brain. Kamber et al. [1992, 1994] have used a similar technique to identify grey/white matter and ventricles in the context of multiple sclerosis lesion identification; however, the model she used

[1]These definitions are used for the following terms in the text: *registration*: the act of aligning two or more data sets to establish a spatial correspondence between represented structures. *non-linear matching*: an instance of registration where correspondence is achieved with a non-linear spatial transformation. *segmentation*: the regional parcellation of an image into anatomically meaningful contiguous groups of voxels. *classification*: the labelling of individual voxels with a tissue class without demanding spatial contiguity for a class of voxels.

was based on MRI data from 12 subjects instead of the single data set used by Zachmann. These two authors used only linear transformations to match the anatomical model to the given data set.

Since there exists a significant amount of morphometric variability between subjects, non-linear transformations must be used to account for fine structure differences persisting after linear registration. One well-known non-linear technique applied to the image matching problem is the thin-plate spline (TPS) algorithm, a manual non-linear warping method based on homologous landmarks [Duchon, 1976; Bookstein, 1989; Evans et al., 1991a]. The procedure decomposes the overall deformation into a series of principal warps of decreasing geometric scale, exactly fitting the manually identified homologous points and interpolating between them. Unfortunately, this type of method has not been practical for routine use as a deformation/warping model because of the subjectivity involved in selecting the precise location and number of points that will define the non-linear deformation.

In other work, idealized geometric models have been used to represent the structures of interest and different warping strategies have been used to deform the model to fit the given data. Many (semi-)automatic methods have used physically based simulated deformations to warp the model to fit the data [Terzopoulos et al., 1988; Nastar and Ayache, 1993]. These objective physically based methods provide a flexible method of deformation, but three problems exist: 1) the modeling of natural phenomena usually results in a deformation that simply finds the nearest local energy minimum, not necessarily the global minimum; 2) the deformation process is modeled as a physical process, which, while perhaps useful in practice, requires that care be taken not to interpret the resulting displacement map as a true physical deformation of the underlying object; and 3) more importantly, only the structure surfaces are represented by geometric models whereas the data to be fitted is a continuous grey-scale field; this mismatch of data type causes problems and can introduce bias in the segmentation process.

The first attempt at intensity-based non-linear registration between two brain data sets was made by Broit [1981], where the atlas was modeled as an elastic object so that it could be physically deformed to match a particular individual's brain volume. This work was continued by Bajcsy and Kovacic [1989] to achieve a multi-resolution solution, based on a coarse-to-fine estimation of local deformations, needed to register the atlas to CT raster data. Their atlas consists of geometrical structure outlines, manually drawn on photographs of macrotomed brain slices. A similar method has been described by Zhengping and Mowforth [1991] to segment MR data, where after linear registration between a voxelated model and data, the model is warped to fit the data. Unfortunately, this method is applied on 2-D slices only, and therefore it can never fully recover the complete non-linear deformation required to match the two volumes together.

Overview of methodology

The following simple example follows the manual segmentation procedure described above and demonstrates the strategy developed in this paper. Suppose a segmented voxel dataset, **A** (for *a*tlas), exists, and that each of its voxels are tagged with some neuroanatomical label. In order to segment another brain volume, **B**, in an equivalent manner, the non-linear spatial warping transformation that optimally maps the intensity field from **A** to **B** must be recovered. Each of the labels in the atlas **A** is then mapped through this transformation onto **B**, thus segmenting **B**. Hence, the segmentation problem is expressed as a registration problem. Implicit in this analysis is the assumption that the first data set is perfectly segmented and that the one-to-one mapping exists. Even though the latter is not strictly true—one brain may have a sulcal pattern that another does not—the assumption does not lead to catastrophic deformations of one structure onto another in practice. The brains are matched at successively finer scales until the assumption of anatomical correspondence breaks down.

In the work presented here, a single MRI brain volume was labelled by a neuroanatomist and serves as the model atlas (the term model will be used in the rest of the paper) in this study.[2] To summarize the automatic segmentation process, we begin by extracting features from the given data set (the *source*) for matching with similar features previously extracted from the model volume. Afterwards, a generic, fully automatic, hierarchical, iterative, non-linear registration procedure (described below) is applied to identify the spatial transformation that, under certain constraints, best registers corresponding image features between the model and the source. The transformation is recovered by detecting the local deformations required to map each region of the model onto its

[2]There exists the possibility of introducing bias in structure segmentation when using a model derived from a single brain which may represent an extreme of the normal distribution. We are in the process of building a multi-subject atlas that will represent the "most average" brain as well as normal anatomical variability [Evans et al., 1992a, 1994]. Nevertheless, the use of a single brain does not change the methodological principles presented here.

homologue in the source data in hierarchical fashion, starting with large regions and reducing their size at each iteration. The largest deformations are recovered first, based on heavily blurred copies of both source and model. The global non-linear warp is built up by summation of smaller deformations determined over the whole volume. Segmentation is then achieved by mapping the atlas labels from the model through this global deformation onto the particular volume.

The segmentation task presented in this paper inverts the conventional approach. Instead of matching atlas contours directly to the image data (as in [Bajcsy and Kovacic, 1989]), features derived from the raster data of both the model and source volumes are used to drive the matching process. Furthermore, all processing for registration and segmentation is performed entirely in *3-D*. This point must be stressed, since the majority of previous work has been completed only in 2-D. Although computationally more intensive, the 3-D algorithms make the problem tractable, since a 2-D procedure can never account for data out of the plane of interest.

The separation of segmentation into a registration followed by delineation yields one powerful advantage over other model-based segmentation methods. This design makes for *atlas-independent segmentation*. The geometric contours defined on the model image volume are not used in any way to determine the match between data and model. The non-linear transformation is established from the raster data in the brain model. Therefore, *any* atlas defined in the model space can be used for segmentation, thereby allowing for the co-existence of multiple atlases, each of which is simultaneously mappable to the native MR image volume without having to recalculate the non-linear matching transformation. For example, functional areas whose edges do not correspond to an explicit anatomical border, but whose limits can be inferred from the underlying anatomical substrate, can be incorporated into the atlas definitions without affecting the algorithm's matching procedure.

METHODS

Image features

Both linear and non-linear registration procedures rely on the extraction of geometrically invariant features from the original volumetric images. We have chosen to use blurred image intensity and image gradient magnitude so that the features are independent of the original position, scale and orientation of one data set with respect to the other. In this way, the magnitude image feature corresponding to a particular anatomical landmark has the same value regardless of its position or orientation within the image volume. These features are calculated by convolution of the original data with zeroth and first order 3-D isotropic Gaussian derivatives. Convolution with such an operator maintains linearity, shift-invariance and rotational-invariance in the detection of features [tar Haar Romeny, 1991; Koenderink and van Doorn, 1987]. This operator is not scale-invariant since the Gaussian kernel is dependent on the standard deviation, σ. We use the full-width-half-max (FWHM = 2.35σ) of this kernel as the parameter to measure the spatial scale.

The optimization procedure used to recover the best spatial transformations are accomplished in a hierarchical multi-scale fashion where the registration is performed at different spatial scales, starting with very blurred data and increasing detail at each step by using less blurred images, refining the registration at each stage. As well as increasing the speed of calculation with respect to performing all operations at the smallest scale (highest resolution), this strategy has the important added benefit of avoiding local minima in the objective function hyper-surface.

Linear registration

Registration of the model with a single source brain volume is accomplished in two optimization steps: the first accounts for the linear component of the transformation function, and the second for the non-linear component. The linear transformation is found automatically by estimating the best affine transformation matrix that maximizes the correlation of invariant features extracted from both model and source volumes and is described in detail in Collins et al. [1994a].

Non-linear registration

In order to account for non-linear morphological differences in normal anatomy between source and model volumes, local deformations are applied to the model volume to improve the alignment of specific regions. These deformations are estimated with a hierarchical multi-scale, multi-resolution strategy. At each step in scale space, the goal of the optimization procedure is to identify the non-linear transformation **D** that maximizes the similarity between features derived from the voxels in the two data sets: the volumetric data for the subject, $\mathcal{V}_s$, and the model, $\mathcal{V}_m$. Using recursive refinement, this optimization procedure is applied to data at different resolutions, beginning with very blurred data so that gross structures

drive the fit at first. The resulting deformation field is then used as a starting point for the next scale step, where less blurred data allow smaller details to be included in processing, thus refining the fit.

The non-linear registration technique developed here is a straightforward extension of the linear registration method, except that the target volume is a small neighbourhood of the whole brain, recursively selected by stepping through the entire target volume in a 3-D grid pattern [Collins et al., 1994b; Collins, 1994c]. The following sections describe the 3-D non-linear registration procedure for a given scale step. We begin by describing the representation of the deformation field. The following sections describe the similarity measure, the constraints and the optimization method used to estimate a local deformation. Implementation details concerning the scale of the extracted features are also addressed.

Deformation field

In the implementation of the ANIMAL algorithm, **D** is represented by a deformation field that is defined on a 3-D cubic lattice, $\mathscr{L}$, with a 3-D displacement vector stored for each node position in the lattice. In practice, three scalar volumes are stored: *dx*, *dy* and *dz*, representing the *x*, *y* and *z*-components of the 3-D displacement vectors. For a given arbitrary (*x*, *y*, *z*) position in the domain of the deformation function, the value of the corresponding 3-D displacement is given by interpolation in each component volume, yielding the three necessary values for the 3-D vector.

The deformation function is recovered hierarchically at a number of different steps, each successive step refining the estimation of the previous one. Each step attempts to recover the deformation function for a given scale corresponding to the resolution of the band-limited deformation function to be recovered. If the FWHM of the current scale step is used to measure resolution, then the voxel spacing of the deformation field lattice must be no greater than FWHM/2 to recover the function without aliasing, i.e., the usual Nyquist sampling limit.

Similarity measurement

The deformation is recovered by estimating the necessary local deformation at each node of $\mathscr{L}$ that maximizes the similarity criterion while satisfying certain smoothness constraints. A correlation coefficient is estimated at each of the lattice nodes using the same principle as the linear registration; however, the correlation is based on a summation over a set of voxels in the local neighbourhood of the particular node. Hence, $R()$ is the normalized correlation value between the local neighbourhood of $\vec{x}$ in $\mathscr{V}_m$ and the corresponding neighbourhood of $\mathbf{N}(\vec{x})$ in $\mathscr{V}_s$:

$$R(\mathscr{V}_m, \mathscr{V}_s; \mathbf{N}, \vec{x}) = \frac{\Sigma_{v \in N_{\vec{x}}} f(\mathscr{V}_m, v) f(\mathscr{V}_s, \mathbf{N}(v))}{(\Sigma_{v \in N_{\vec{x}}} f^2(\mathscr{V}_m, v))^{1/2} (\Sigma_{v \in N_{\vec{x}}} f^2(\mathscr{V}_s, \mathbf{N}(v)))^{1/2}}, \quad (1)$$

where **N** is the current estimate of the model to source transformation, $N_{\vec{x}}$ is the local neighbourhood of $\vec{x}$ with diameter = ½FWHM, $f(\mathscr{V}, u)$ is the interpolated feature value from the volume $\mathscr{V}$ at voxel position v, and the summation is performed over all voxel elements $v \in N_{\vec{x}}$. A local neighbourhood diameter of 1.5FWHM was empirically chosen since a diameter of 1.0FWHM, initially used to allow complete coverage in areas subject to expansion or stretching and to maintain continuity of the deformation field, was shown to be insufficient. The value of 1.5FWHM was the smallest diameter that resulted in robust estimation of deformation vectors. Larger diameters such as 2.0FWHM or 2.5FWHM enforce greater continuity between regions at the expense of possibly missing small local deformations.

The local neighbourhood of $\vec{x}$, $\mathscr{N}_{\vec{x}}$, is defined by a sub-lattice of nodes. For data blurred at a scale of FWHM, it is necessary to have samples spaced at FWHM/2 to recover the underlying band-limited blurred intensity function, yielding a 3 × 3 × 3 neighbourhood. Twice as many samples (in each direction) are required to fit the gradient data, since the gradient magnitude changes at a twice the rate of the blurred data. Therefore, the local neighbourhood is defined on a 7 × 7 × 7 region.

The normalized similarity value, *S*, between the two volumes, $\mathscr{V}_s$ and $\mathscr{V}_m$ for a given transformation **N** is defined as the sum of all local correlations:

$$S(\mathscr{V}_m, \mathscr{V}_s; \mathbf{N}) = \frac{1}{n} \sum_{\vec{x} \in \mathscr{L}} R(\mathscr{V}_m, \mathscr{V}_s; \mathbf{N}, \vec{x}), \quad (2)$$

where n is the number of elements in $\mathscr{L}$. R, and likewise S, take on a maximum value of 1.0 when the two volumes are in perfect registration.

Estimation of local deformation

It is clear that equation 2 is maximized when each of the terms in the summation are at a maximum. Since the transformation **N** is stored such that there is one

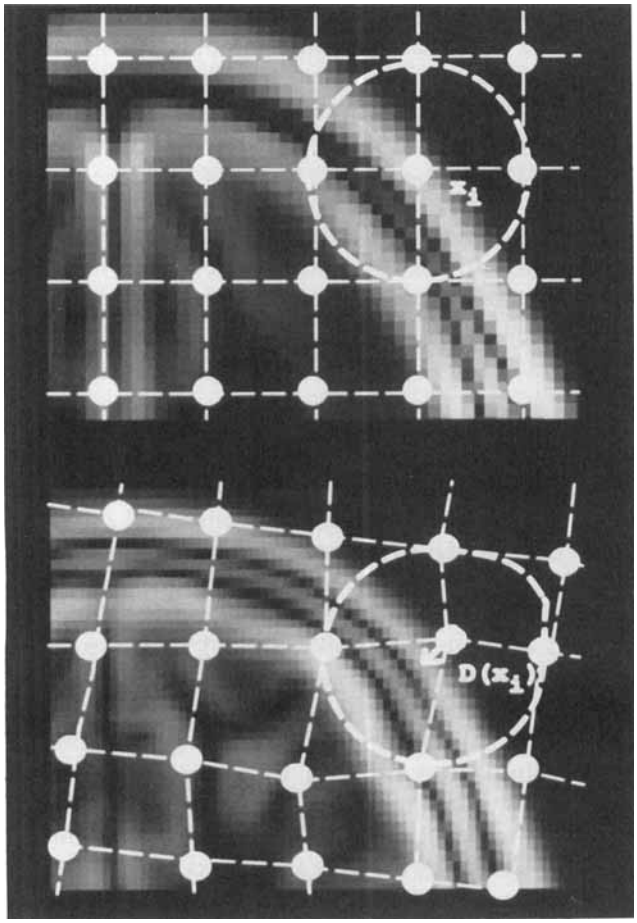

Figure 1.
Non-linear registration strategy. The images show part of the 3-D lattice overlaid on the gradient magnitude data. Under the current transformation, the node x_i is mapped to $D \cdot (x_i)$ on the model. A small displacement (indicated by the arrow) towards the edge of the scalp is necessary to maximize the neighbourhood correlation for this node. This is found through optimization of the three translational parameters (dx, dy and dz).

deformation vector for each node $\vec{x}$, equation 2 is maximized by optimization at each node of $\mathscr{L}$. The optimization is similar to that performed for the linear registration procedure; however, only three parameters are optimized instead of nine, since only three are required to define the local deformation vector $\vec{d}_i$ that maximizes for correlation of the local neighbourhood of $\vec{x}_i$ with its homologue in the target volume. Hence, the goal is to find $\vec{d}_i$ that maximizes $R(\mathscr{V}_m, \mathscr{V}_s; (\mathbf{N} + \vec{d}_i), \vec{x}_i)$. (See Fig. 1.)

The local neighbourhood of $\vec{x}_i$ is specified by the ensemble of interpolated feature values from each sub-lattice node defined above. Before optimization, the corresponding neighbourhood in the target volume is defined by transforming each sub-lattice node by the current non-linear transformation **N** and interpolating the feature value on the target volume. The vector $\vec{d}_i$ is found using a three-dimensional Simplex optimization procedure, maximizing the correlation between the two sub-lattices.

Smoothing constraints

Since a continuous deformation field is required, the estimation process must be constrained so that it cannot compress two distinct points together or allow an overlap, nor can it induce a tearing of the field. This is achieved by tempering the deformation vector above with the average of the deformation vectors of the neighbouring nodes. If $\mathbf{M}(\vec{x})$ is the mean deformation vector calculated from the immediate neighbourhood of $\vec{x}$, then the resulting deformation is given by:

$$\vec{d}' = \alpha\vec{d} + (1 - \alpha)\mathbf{M}(\vec{x}) \qquad (3)$$

where $0 \leq \alpha \leq 1.0$. A small value of α ensures a very smooth deformation field at the expense of possibly missing some small local variations, while a large value of α gives more importance to the estimated deformation vector, with the risk of permitting local discontinuities to pass into the global deformation field. We have found that $\alpha = 0.5$ yields an acceptable balance between local matching and global smoothness.

Scale of local neighbourhood features

The estimation of a local deformation vector is based on the correlation of image-intensity gradient-magnitude derived from both the source and target volumes. Since gradient extraction is dependent on scale, this parameter must be chosen in relation to the scale of the estimated deformation function. A very large value is of no use, since it will blur out important structural detail from the volumetric data, while a very small value will extract a lot of structure, increasing the probability of local mismatches. The size of the Gaussian blurring kernel applied to the volumetric data was chosen to be equal to the resolution of the deformation field estimated at the current scale step. Scale factors yielding gradient magnitude data with twice the resolution and with half the resolution were also tried. Only small differences in the recovery of the deformation field were observed, when compared to when the gradient magnitude data was at the same scale.

Iterative refinement

Since the deformation at a single node is part of a continuous global warp, it affects not only that node, but all neighbouring nodes as well. The correlation values for those neighbouring nodes will also change as a result. Consequently, an iterative approach is used, where a fractional value of the estimated deformation is stored for each node at each iteration. Experimentally, we have found that a fractional value less than 0.3 yielded very robust results; however, too many iterations were required to be practical. While values greater than 0.75 converged quickly, an incorrect match at one node could pull neighbouring nodes from their correct location. We have selected a value of 0.6 as a compromise between robustness and speed of convergence. At this level, we have found that only four to six iterations are needed at each scale.

Since the optimization procedure terminates sooner when the initial conditions are close to the final result, and since calculating the fit at one scale requires less than one-quarter the time taken for the fit at half that scale, more iterations are allowed for the first two resolution steps: 15 iterations at 24mm scale and 10 at 16mm scale.

Hierarchical operation

The preceding sections have described the methodology used to estimate the deformation field for a given scale-step (or resolution). The overall estimation requires multiple fits in decreasing scale (increasing resolution), each successive step refining the fit of the last. The smallest scale of the deformation is dictated by the resolution of the data used in the estimation, and the largest by the field of view. A factor of 2 was initially used to step through scale space, starting at the original pixel size and sampling at 2, 4, 8, 16 and 32 times the original pixel size. It was found that scales of 32mm and greater blur the data too much to be of any use in the estimation of the deformation, so the non-linear registration procedure begins by estimating the deformation field on data blurred with a 24mm FWHM Gaussian kernel. The spacing between lattice nodes is 12mm at this scale. Resampling the data through the transformation at this scale shows that the overall fit is greatly improved as the basic brain shape is recovered and matched. A single iteration at this scale, estimating local deformations at each node of the 3-D lattice, requires 1 minute to compute on a SGI Indigo^2 Extreme (60.5 SpecFP Unix machine).

After completion, the 24mm scale deformation field is resampled onto a 3-D lattice with 8mm spacing and used as input for the refinement of the deformation field using data blurred with a 16mm FWHM Gaussian kernel. Each iteration requires 4 minutes computation time for a total of 40 minutes at this scale. At this point, the individual lobes and the major sulci have come into correspondence between source and model volumes. Depending on the application, the process can stop at this point or continue decreasing scale (increasing resolution) with data blurred at 8mm, 4mm and 2mm for a finer fit and longer run times (see Fig. 8).

Segmentation

The segmentation procedure described in this paper depends on a two-part design for the model volume. The model consists of, first, image data, and, second, a set of atlas labels defined voxel-per-voxel over the image data. Initially, the source volume is registered with the model volume to obtain a forward spatial transformation. Subsequently, the atlas label volume is mapped through the inverse spatial transformation, thereby labelling the source volume.

As this segmentation is independent of the image data and initial registration, *any* atlas defined on the target volume can be used to segment the source volume. As anatomical nomenclatures and usages vary, a suite of atlases can be defined in the model space to allow users to select a nomenclature of choice. These atlases could range from any of a number of standard neuroanatomical atlases (Schaltenbrand and Bailey [1959], Ono et al. [1990], Talaraich and Tournoux [1988]), to Brodmann's [1909] or von Economo's [1929] cytoarchitectonic regions or Flechsig's [1896] myeloarchitectural regions. As well as providing for different nomeclatures, the atlases defined over the model can have a variety of natures, ranging from manually segmented anatomic structures (as presented here) to maps of brain function.

EXPERIMENTS AND RESULTS

Experiments are presented using three types of data: a simple geometric ellipsoid phantom, a realistic digital brain phantom and real 3-D MRI data of 11 normal volunteers.

Ellipsoid phantom

A simple volumetric brain phantom was created to demonstrate the feasibility of the segmentation strategy. The phantom contains three concentric ellipsoids representing the skin surface, cortical surface and grey-white interface, and two smaller ellipsoids to

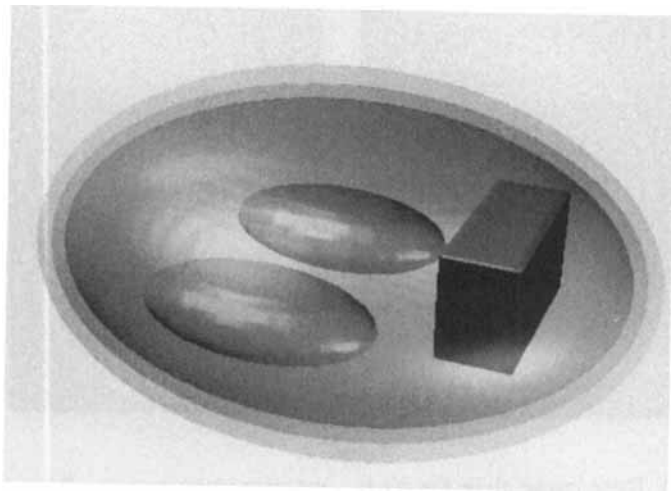

Figure 2.

3-D rendering of ellipsoid phantom. The simple ellipsoid phantom contains two large concentric ellipsoids to model the cortex and grey/white matter interface. Two smaller oblong ellipsoids represent the lateral ventricles. This phantom is used to demonstrate the ANIMAL algorithm. Note that while 2-D images are shown in Figures 3 and 4, all data is volumetric and all processing is completed entirely in 3-D.

represent the ventricles. The parallelepiped represents an arbitrary structure within the phantom. The long axis of the phantom is 100mm in length, and it was generated in a volume with a 128 × 128 × 128 matrix, with 1mm^3 voxel size. Figure 2 shows a 3-D rendering of the phantom. A manually defined TPS [Bookstein, 1989; Evans et al., 1991a] warp was used to deform the phantom and create a warped target. The ANIMAL algorithm was then applied to fit the original volume onto its warped counterpart. The geometric contours defined on the original phantom were mapped through the recovered non-linear transformation and overlaid on the target data set. Figure 3 shows the resulting segmentation for the linear transformation and the first, third and last scale steps (24mm, 8mm and 2mm) of the non-linear transformation. There is a significant improvement in segmentation evident at the first non-linear result when compared to the linearly transformed contours. The successive steps in scale refine the segmentation even further, finishing with an almost perfect segmentation of the phantom.

Two quantitative error measures are used to evaluate the quality of the segmentation. The first simply measures the percent difference in absolute volume between the true and the segmented structure. This value is defined as:

$$\delta(T, S) = \frac{V_T - V_S}{V_T} \times 100.0\%, \tag{4}$$

where δ is the percent difference in absolute volume, V_T is the volume of the true structure and V_S is the volume of the automatically segmented structure. While this value indicates differences in size between the segmented and true structures, it does not measure the quality of the segmentation, since two structures can have the same volume and not be the same shape, or be in the same position. The second error measure is the percent volume overlap, Δ, defined as:

$$\Delta(T, S) = \frac{|T \cap S|}{|T|} \times 100.0\%, \tag{5}$$

where T is the set of voxels in the true structure, S is the set of voxels in the automatically segmented structure, $\cap$ indicates volumetric intersection and $|\cdot|$ returns the volume of the set of voxels. This value equals 100.0 when the segmented and true structures completely overlap. In fact, if the segmented structure is larger than the true structure, Δ can still equal to 100.0. Therefore, one measure forward $\Delta_f = \Delta(T, S)$ and one measure backward $\Delta_b = \Delta(S, T)$ were calculated, and the minimum of the two was used to estimate the segmentation results.

The five objects used in the definition of the ellipsoid phantom were assessed individually. For the segmentation described above, the values of δ and Δ were calculated for each object. The results in Table I show that on average the estimated segmented struc-

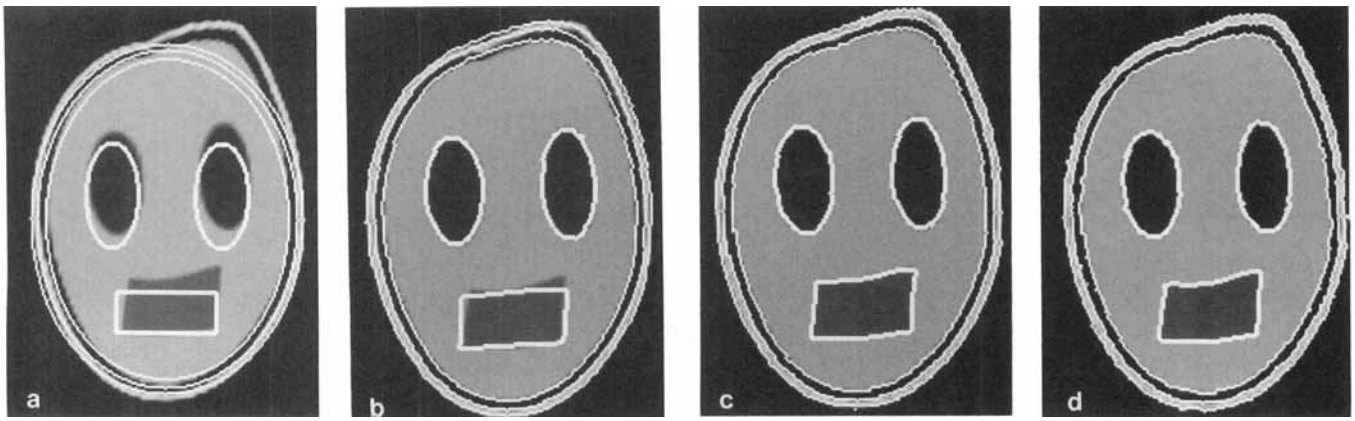

Figure 3.

Segmentation of ellipsoid phantom. These images show the result of the segmentation procedure applied to the ellipsoid phantom. From left to right, the ellipsoid contours are mapped through the linear, and the first, third and last scale steps (24mm, 8mm and 2mm) of the non-linear transformation. The first non-linear step begins to take account of the general brain shape, and finds the positions of the ventricles. By the third step in scale, the upper right region of the volume is almost properly segmented as well as the corners of the "mouth"; however, there appears to be a misregistration of approximately 1mm between the object edge and the segmented contour. This error is corrected, and a near-perfect segmentation is completed by the last scale step.

ture volume has less than 1% error and structure overlap is better than 99%.

Brain phantom

A more realistic evaluation of the automatic segmentation employed a digital brain phantom created by identifying different structures and tissue types from an MR data set of a single volunteer. The volume is sampled on a $1\times1\times1mm^3$ matrix, and covers the entire head. The resulting labeled volume could then be endowed with the appropriate contrast for each tissue type, and Rayleigh noise added, to resemble a true MR acquisition. This 3-D data set provides a gold-standard with which to evaluate the ANIMAL registration algorithm. It should be noted that it does not matter that some voxels from the original MRI data may have been mislabeled. The labeled volume is now a phantom defined as *truth* and is no different in principle than the arbitrarily defined ellipsoid phantom. It has the advantage that it is a geometrically complex simulated data set which closely mimics the convoluted nature of a real brain and whose intensities and noise characteristics match those dealt with in MRI.

TABLE I. Segmentation results for ellipsoid phantom

	Linear		Non-linear	
Structure	δ	Δ	δ	Δ
Skin	7.1%	92.8%	−0.2%	99.9%
Brain	6.1%	93.4%	0.6%	99.6%
Ventricle (R)	1.7%	84.8%	0.5%	99.3%
Ventricle (L)	−2.1%	77.3%	0.5%	99.1%
Rectangle	23.0%	71.1%	−1.9%	98.3%
Average mag	8.0%	83.9%	0.7%	99.2%

This table shows the percent volume difference, δ, and the percent volume overlap, Δ, for the individual structures used to define the ellipsoid phantom. These values are normalized to the true structure volume.

A set of landmarks was chosen to produce a TPS transformation that was applied to the 3-D T1-weighted phantom data set to produce a topographically equivalent, but spatially warped target data set. Ten percent noise, corresponding to the signal-to-noise ratio of our scanner, was added to the source volume.

The voxels contained in five anatomical structures (head of left and right caudate, lateral and third ventricles) were manually identified on the original unwarped phantom data using a voxel painting feature within a software program, developed at the MNI, that allowed simultaneous real-time tri-plane (transverse, coronal and sagittal) viewing of volumetric data. These structures were then mapped through the applied transformation to create a corresponding set of known structures in the warped data volume. (These are the structures that must be segmented by ANIMAL.)

The set of five unwarped/warped structures were used to evaluate the ANIMAL algorithm using the

percent difference and the percent overlap measures defined above. The contours defined by the painted structures were mapped back through the inverse of the recovered transformation and overlaid on the warped data. As Figure 4 shows, as an enlarged portion of a 2-D slice though these contours, the structures in the segmented data are outlined well by the warped contours.

Since a preclassified data set was used to create the brain phantom, the set of grey-matter and white-matter voxels were known and the overlap indices could be evaluated in the same way for the tissue classes as for the brain structures. Table II shows that on average, δ was reduced by more than half, from 4.2% to 1.7%, and Δ was improved, from 70.4% to 97.0% when comparing non-linear to linear matching.

In order to assess the quality of the non-linear registration based Δ in terms of misregistration distance, a single caudate was taken and deliberately misregistered by applying a translation along one of the three axes. The value of Δ was calculated for each original/misregistered pair for offset values varying from -5mm to 5mm, in steps of 0.25 mm along the x, y and z coordinate axes. The results are shown in Figure 5. The volumetric correlation on intensity values was calculated as well and plotted for comparison; Δ corresponds well with the correlation coefficient at each offset position. A value of Δ greater than 90% corresponds to less than 1mm misregistration along the x-axis. The same misregistration on either the y or z axes alone corresponds to a Δ of approximately 95%. Therefore, the value of 96.4% found for caudate in this experiment indicates that there is less than 1mm misregistration in the segmentation of the simulated data.

Since the recovery of the applied deformation was quite good for 10% noise, one may ask what is the behavior of the non-linear registration algorithm in the presence of greater levels of noise. Using the

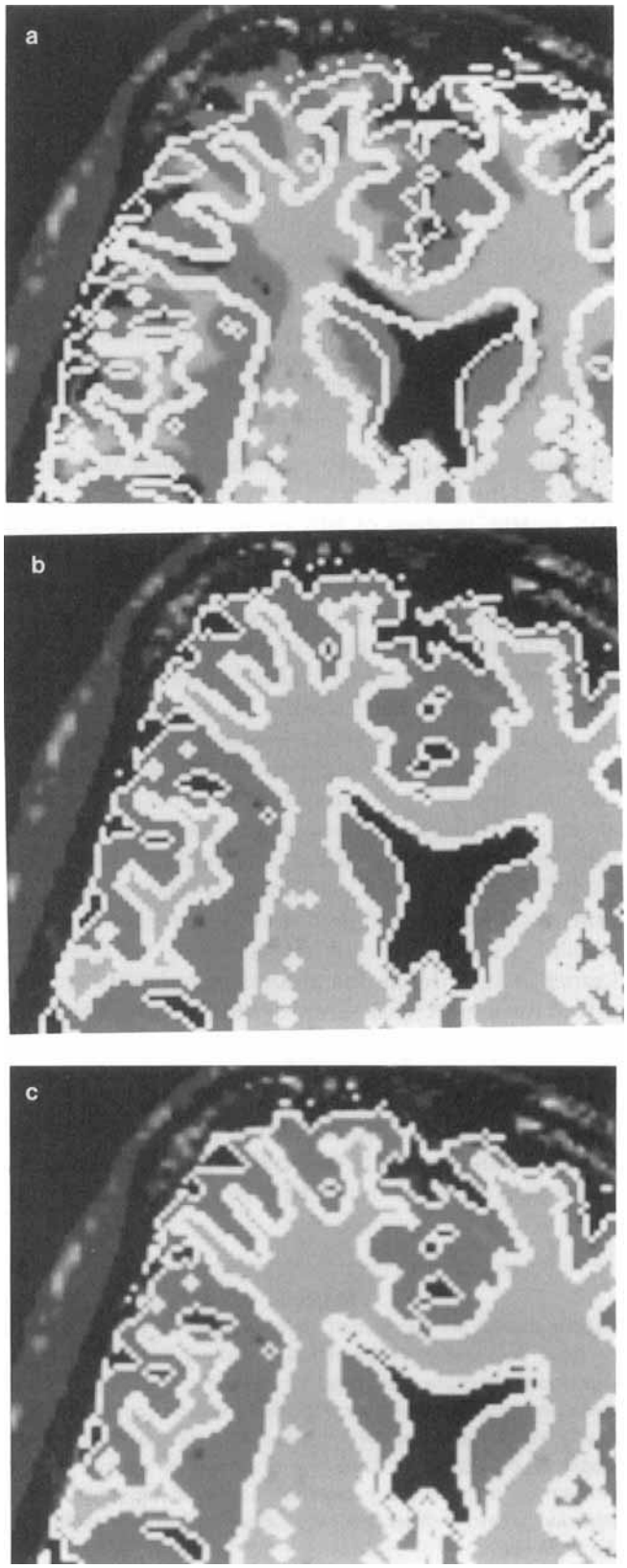

Figure 4.
Segmentation of digital brain phantom. Three transverse images of the 3-D digital brain phantom through the ventricles at the level of the basal ganglia are shown here with the contours of the resulting segmentation superimposed. The contours correspond to the head of caudate, the lateral ventricles and the grey and white matter boundaries. On the left, the contours are mapped through the linear transformation only. In the center are the true contours, generated by mapping the original atlas contours through the known TPS transformation. On the right are the contours resulting from the ANIMAL segmentation. Almost no difference is visible between the two sets of contours.

TABLE II. Segmentation results for brain phantom

Structure	Linear		Non-linear	
	δ	Δ	δ	Δ
Caudate	1.3%	65.7%	4.9%	96.4%
Ventricle	7.0%	77.6%	−0.0%	99.1%
Grey	3.4%	72.0%	1.0%	97.0%
White	5.0%	66.1%	−0.7%	95.6%
Average	4.2%	70.4%	1.7%	97.0%

This table shows the percent volume difference, δ, and the percent volume overlap, Δ, for the individual structures defined on the digital brain phantom and segmented from a manually warped data set. These values are normalized to the true structure volume.

T1-weighted images, Rayleigh distributed noise was added to the unwarped source volume at levels from 10% to 80% in steps of 10% of the non-zero signal of the input volume. Since the non-linear transform used to create the target volume is known, the difference between the applied and recovered transformations can be measured. The *recovery error* is defined to be the root mean squared (r.m.s.) value of this measurement, evaluated over all brain voxels. As shown in Figure 6, the algorithm is very stable throughout the range of noise levels tested, ranging from 0.62 ± 0.59mm for 10% noise to 0.85 ± 0.66mm for 80% noise. Therefore, at the levels of noise expected in typical MRI volumes (i.e., less than 10%), these simulations show that ANIMAL recovers the non-linear spatial transformation required for segmentation. The reason for this stability is due to the inherent blurring of the Gaussian kernel used to define the gradient magnitude feature and to the hierarchical nature of the estimation process.

Human MRI data

Eleven normal volunteers (29 ± 3 years old; 10 males, 1 female; 9 right-handed, 2 left-handed) were scanned in a Philips Gyroscan ACS 1.5 Tesla supercon-

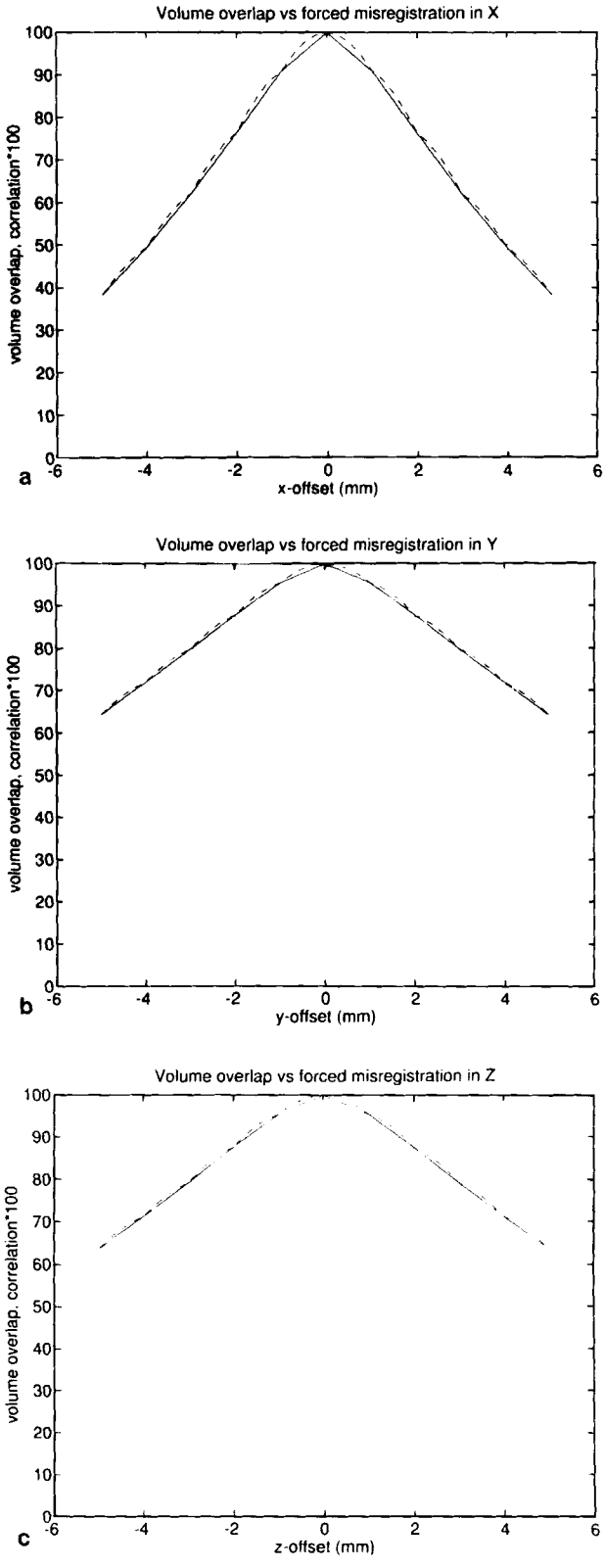

Figure 5.
Volume overlap and correlation value vs. registration error. Plot of △ (solid line) and correlation value (dashed line) for a single segmented structure (left head of caudate). The data set was deliberately misregistered, varying one translation component (x, y or z) at a time. Note that the graph for x-offset is steeper due to the shape of the caudate. Since the structure is narrow in the x-direction, taller in the y direction and even longer in the z direction, a 1mm x-offset reduces △ more that an y- or z-offset of the same size.

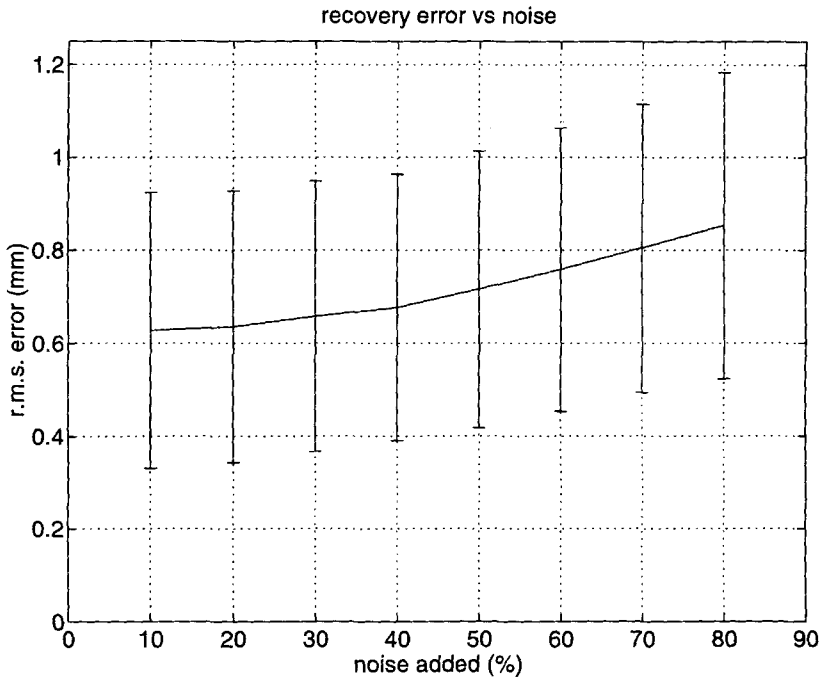

Figure 6.

ANIMAL behavior in the presence of noise. This graph shows the behavior of the algorithm as described by the recovery error, the *r.m.s. difference in deformation* between the applied and recovered transformation for all brain voxels. The tick marks indicate 1 SD.

ducting magnet system for the experiments described below. The data were acquired with a T1-weighted 3-D spoiled gradient-echo acquisition with sagittal volume excitation (TR = 18, TE = 10, flip angle = 30°, 140–180 sagittal slices). This sequence achieves a high grey/white matter contrast with good signal-to-noise characteristics (15:1). For the purposes of this article, we assume the volumetric data to be artefact-free since a number of algorithms exist to minimize the effect of artefacts from the volumetric data.

For validation of the ANIMAL algorithm on real data, a set of structures were defined by hand on the 11 data volumes. The voxel painting program described above was used by a trained neuroanatomist to identify individual anatomical structures in these brain volumes. The voxels labeled by this procedure serve as the gold-standard definition for each structure on each brain. Six structures were chosen for testing, some because of their inherent importance in many aspects of current brain research and because they present relatively well-defined objects for manual labeling: the left and right head of caudate, the left and right lentiform nucleus (globus pallidus and putamen) and the two lateral ventricles.

Without loss of generality, the ANIMAL algorithm allows one brain to serve as a model and structures identified on it to define the anatomical atlas that is used for segmentation of all other data sets. Therefore one brain volume, and its associated voxel labels, were selected as the model and the other ten data sets segmented automatically by automatic non-linear registration to it.

After application of the ANIMAL algorithm to each of the individual/model pairs, the inverse of the recovered transformation was used to resample the structure labels of the target volume onto the individual data set. Figure 7 shows three transverse slices through the ventricles and basal ganglia of one of these segmented data sets. Contours corresponding to the head of caudate, lentiform nucleus and the lateral ventricles are overlaid on the images for both the manual and automatic segmentation. Comparison of the two sets of images shows that the ANIMAL algorithm succeeds in identifying the boundaries of the structure, based on its definition in the model brain.

The results in Figure 8 show how the values of δ and Δ change with increasing scale step. Table III shows

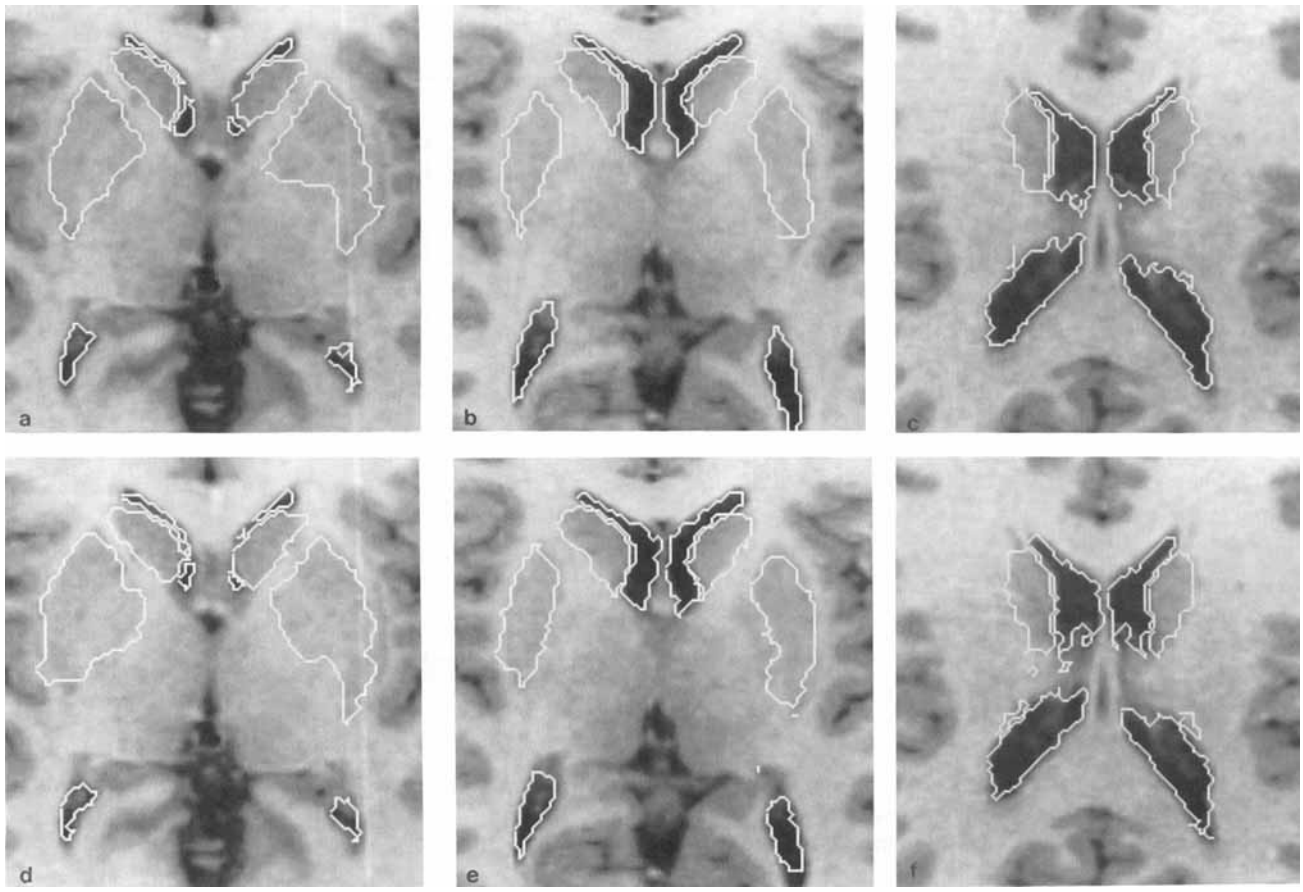

Figure 7.

Typical segmentation of real MRI data. Transverse slices through a single brain at the level of the ventricles and basal ganglia. The manually identified contours for the caudate, lentiform nucleus and ventricles are shown in the top row. The corresponding automatic segmentation (scale = 2mm) is shown in the bottom row. Notice that there is good agreement between the manually and automatically defined contours.

that the overlap increases from 67% to 87% on average over the six structures defined on the ten subjects, for the segmentation achieved with the 2mm scale deformation field. The percent volume difference of the right caudate is greater than in the left, after nonlinear segmentation. Since the right caudate is thinner and occupies slightly less volume than the left (5285mm^3 vs. 5482mm^3, on average of the manually segmented data), misregistration between the automatic and manually segmented structures cause more important errors for the right side. It is interesting to note that after linear registration, the value of δ is quite large, and Δ indicates an overlap of slightly better than 50% for the ventricles, due to the large amount of anatomical variability for this structure. The nonlinear registration results show that the ANIMAL procedure can capture and remove this variability. While the value of Δ increased to more than 97% for the simulations using the brain phantom (Table II), Δ increases to 85–90% with real data. There are three reasons for this lack of improvement:

1) Intra-subject intra-observer variability: Recall that in the brain phantom simulations, the target structures to be segmented are based on their definition in the source volume and the applied transformation. By definition in the simulation, the target structures are simply the original structures transformed by the applied transformation. The automatically segmented structures are defined to be the original structures *transformed by the recovered transformation.* Thus, it is only the difference between the applied and recovered transformations that gives rise to non-null values of δ and values less than 100% for Δ. Only a single manual intervention is needed to identify the structures, and thus intra-observer variability plays no role in the brain phantom simulations. For experiments in real MRI data, structures in both the source and target volumes are identified manually and intra-observer

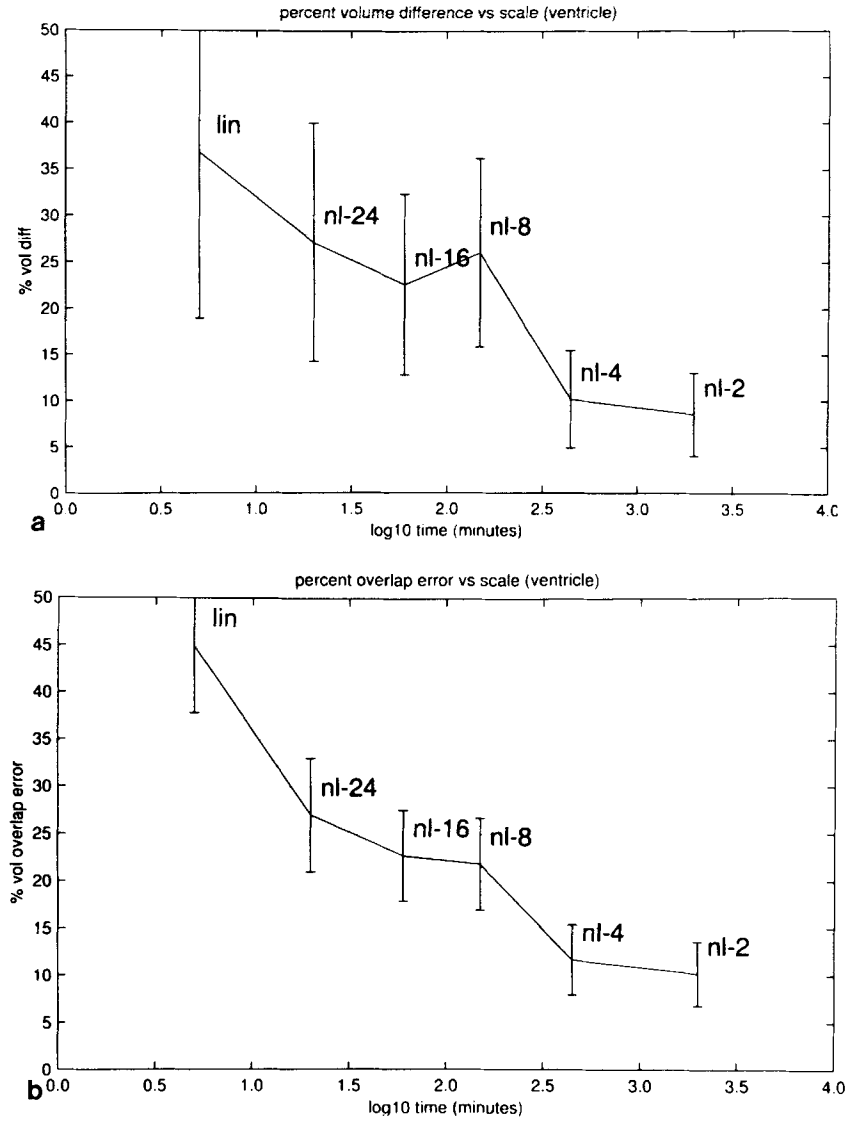

Figure 8.

Volume difference and overlap error for segmentation of ventricles vs. time. The top graph shows the value of $|\delta|$ as a function of computation time averaged over ten brains for the automatically segmented lateral ventricles for the linear transformation (lin) and the non-linear transformation at scales of 24mm (nl–24), 16mm (nl–16), 8mm (nl–8), 4mm (nl–4) and 2mm (nl–2). The height of the tick marks represents 1 SD on the mean magnitude of δ. The bottom graph shows the value of 100% − Δ for the same data. The first non-linear registration step requires 15 minutes and the second, 40 minutes. The time per iteration increases by a factor of approximately four for each additional scale step.

variability becomes important. Since manually identified structures are used for the "gold standard," how good is this standard? In a simple anecdotal experiment performed to provide a point of comparison, the anatomist manually segmented the left and right caudate on the same subject on three occasions over a 3-month period. The average magnitudes of δ and Δ were 4.9% and 87.8%, respectively. These values impose a limit on the quality measure and we can conclude that the ANIMAL segmentation is comparable with manual results.

2) Inter-subject intra-observer variability: Anatomical differences between subjects complicates the manual segmentation process. For example, the lentiform nucleus is composed of the large lateral putamen and smaller medial globus pallidus. The central lenti-

TABLE III. Segmentation results for real MRI data

Structure	Linear		Non-linear	
	δ	Δ	δ	Δ
Ventricle (R)	47.4%	52.8%	10.0%	89.5%
Ventricle (L)	33.2%	55.9%	7.8%	89.7%
Caudate (R)	10.6%	71.2%	12.3%	83.3%
Caudate (L)	9.5%	68.5%	8.2%	85.5%
Lentiform (R)	8.6%	77.5%	7.0%	85.1%
Lentiform (L)	6.6%	76.7%	6.4%	86.7%
Average	21.1%	67.1%	7.9%	86.6%

Percent volume difference, δ, and the percent volume overlap, Δ, for the individual structures segmented manually and automatically. These values are normalized to the manually identified structure volume.

form nucleus is easily distinguished from the surrounding white matter of the internal capsule. Laterally, however, the lentiform nucleus is bounded by the external capsule and claustrum, whose combined width may reach a maximum of 5mm but is more likely to be on the order of 1–2mm. This makes the regular distinction of the lateral boundary difficult. The putamen itself narrows considerably both rostrally and caudally. These fine edges that are often intermingled with fibre bundles and are unclear in many sections. Ventrally, the histologically similar substantia innominata and other basal forebrain regions do not provide clear boundaries for the lentiform nucleus in MRI, except at the level of the anterior commissure.

Overall, the caudate nucleus is an uncomplicated structure to draw. Rostrally, the head of the caudate is a large elliptical structure with discrete boundaries. There is a sharply contrasting border medially with the CSF of the lateral ventricle and laterally with the white matter of the anterior limb of the internal capsule. Ventrally, there is no clearly defined boundary between the caudate and putamen (which are the same structure in the histological sense). This makes the ventrolateral boundary an arbitrary distinction. Caudally, the tail of the caudate decreases in size to a dimension on the same order as the voxel resolution. The proximity of the thalamus and hippocampus (in the temporal lobe) makes observation of the caudate in this area difficult or impossible. These difficulties may cause variabilities of up to 5% in the definition of the structures.

3) Model bias: The third cause of error is bias incurred by using the manually segmented structures from a single individual for the model atlas. Any errors in that single manual segmentation are carried through the non-linear transformation, yielding errors in the segmentation. This will be true in general for any atlas defined on the basis of a single brain.

DISCUSSION

The essential problem in neuroanatomical structure delineation from images is to establish a correspondence between image data and model volume. The major difficulty is due to normal anatomical morphometric variability that causes important structure differences between a single subject and the atlas, or between subjects. The difficulties are compounded when using any imaging technique, which yield degraded poor representations of the underlying anatomy, and thus suffer from low tissue contrast, partial volume effects and misorientation of the scanned slices with those in standard atlases. In the method presented here, segmentation is achieved by non-linear 3-D spatial normalization between data and model.

Both analytic and numerical methods have been proposed in the literature to solve for the non-linear spatial warping function. In analytic approaches, the deformation field is expressed as a weighted combination of pre-defined deformation modes, e.g. as scaling factors along a set of radii or as a weighted sum of basis functions. The main advantages of these techniques (e.g., [Bookstein, 1989; Lemoine et al., 1991]) are the speed at which the transformation can be recovered and the economy of representation of the deformation. This rapidity is achieved at the expense of constraining the space of possible solutions by limiting the number of degrees of freedom. This approach may be perfectly acceptable for some types of analysis where anatomical registration of fine structure is not critical (e.g., image alignment for functional image analysis). However, the accurate structural segmentation discussed here requires almost unlimited degrees of freedom to achieve acceptable delineation of individual brain regions and this justifies the increased computational demands of a full ANIMAL procedure. Of course, this procedure can be terminated at any coarser scale if a fast approximate solution is sufficient. We have chosen to represent the non-linear transformation as a deformation field, where each vector-valued voxel defines the local deformation at each point in the volume. Analysis of the recovered deformations permits the creation of voxel maps of local anatomical variability which can act as stiffness parameters for any future fit. It may also serve in the determination of local neuroanatomical variabil-

ity basis functions that could be used in future analytic fitting techniques.

The procedure requires less than 10 minutes to calculate the 3-D non-linear transformation at the first scale step (FWHM = 24mm) and 40 minutes is required to have a local deformation vector estimated every 8mm throughout the brain volume. Finer resolutions are not needed for inter-subject analysis of functional images that depends on volumetric averaging of PET data, for example. Basis function methods implicitly impose similar filters on the spectral frequencies existing in the deformation field through the spatial frequencies of the allowed basis functions.

In warping techniques based on landmark matching [Duchon, 1976; Bookstein, 1989; Evans et al., 1991a], correspondence is defined explicitly by manually defining homologous points. Problems arise with these methods due to the effects in the choice of number and location of landmarks and the subjective error in identifying equivalent landmarks in different brains. In the automated method presented here, explicit point-to-point correspondence is not required. Where there are no edges (e.g., in a homogeneous region) to estimate a displacement, the deformation vector is interpolated from neighbouring regions.

While the assumption that there exists a 1-to-1 correspondence between two brains is never strictly true, the validity of this assumption depends on the spatial scale of comparison. When blurred at 16mm FWHM, all structures of the brain are topographically equivalent because only major structures (temporal lobe, ventricles, longitudinal fissure) are apparent. This procedure can be applied to blurred data of the whole brain volume to correct overall shape (as if all brains were forced to fit inside the same skull). Smaller features are simply not visible, and do not take part in the estimation process. For the data sets tested, a 1-to-1 mapping could be found between the representations of the primary sulci and gyri as seen in the gradient magnitude data at the 8mm scale even though the topology is not necessarily consistent when seen at the highest resolution (or as shown in the atlas of Ono et al. [1990]). At scales smaller than 8mm, this method is still able to register structures as long as there is a 1-to-1 mapping between them such as the ventricles, basal ganglia and major sulci. In the experiment with the brain phantom where correspondence is guaranteed, the application of ANIMAL yielded successful grey matter segmentation (see Fig. 4): δ improved from 3.4% to 1.0% and more importantly Δ improved from 72% to 97%. For the cortex between different subjects, however, the topology is not consistent for secondary and tertiary gyri [Ono et al., 1990]. This is a completely different problem, complex enough to warrant a separate research project. A solution to this problem has been proposed in our laboratory by MacDonald et al. [1994] where the cortical surface is extracted and mapped onto a simple parametric space with the same topology, e.g., a sphere.

Strengths and weaknesses of the ANIMAL algorithm

The following are believed to be significant contributions made by this paper: 1) a formalism has been developed that can be used for both a) automatic segmentation and b) spatial standardization of volumetric data; 2) atlas-independent segmentation by re-posing of the model-based segmentation paradigm into one involving a registration step followed by a delineation step; 3) removal of the extra level of abstraction in common segmentation methods; instead of directly fitting geometric constructs to raster data, the MRI data is fit to similar features of the model. 4) experimental validation of the linear, non-linear and segmentation methods with simulated phantom data and real MRI volumes; 5) a tool that will yield insights into the extent of morphometric variability in the normal adult population.

The application of the algorithm to pathology is a major extension that has not yet been examined, nor have any attempts been made to address the complications brought about by pathology within the otherwise normal anatomy. Nevertheless, the region of a tumour could be masked by hand so that deformation vectors are not estimated within the mask since there are no corresponding "tumour" structures in the model. After all deformations for non-pathological anatomy are estimated, the deformations for the tumour region could be extrapolated from the neighbouring normal anatomy.

Other applications

The development of an automated 3-D non-linear registration procedure has direct utility in studies of functional neuroanatomy with macroscopic imaging techniques such as PET and fMRI. For PET, averaging across subjects in a standardized space is used to detect subtle cognitive activation foci measured from cerebral blood flow (CBF) volumes [Fox et al., 1985]. The removal of the non-linear individual neuroanatomical differences will potentially remove the blurring due to morphometric variability and potentially increase the signal-to-noise ratio, and enhance the detectability of even smaller signals.

This method could also be directly applicable to the quantitative study of neuroanatomical variability in the normal population, the determination of inter-group differences, the detection of subtle abnormalities, and the tracking of normal development. Furthermore, the application of the ANIMAL procedure yields a volumetric deformation field, where a vector is stored at each voxel location representing the amount of extra deformation needed to match a point from the source to the target. For a given subject, each voxel of the deformation field represents the magnitude and direction of the deformation vector needed to locally match the source to the target after affine transformation. If the target is defined in a standardized space (e.g., the stereotaxic space of Talairach and Tournoux [1988]), then the recovered deformation fields, when averaged over a large number of subjects, quantify the normal anatomical variability for every location in the model space.

Future work

There are two main directions that will be taken in the field of non-linear warping for brain mapping. The first concerns the determination of the best similarity function used to establish correspondence between homologous regions within the source and target volumes. Correlation is only one of many possible similarity functions and is justified when there exists a simple linear mapping between intensity feature values between source and target, as is the case here. The "variance of ratios" minimized by Woods et al. [1993] for intra-subject inter-modality registration is justified when there exists a 1-to-1 mapping between intensity feature values. Recent developments by Collignon et al. [1995] suggest that even more general similarity measures may be possible to allow a T1-weighted target to be used to segment a T2-weighted or even a CT data set. Furthermore, it may be possible to pre-classify the image volume and thus achieve modality-independent non-linear registration. Even though this brings us a step away from the original data and creates a dependency on the classification algorithm, the segmentation results using the brain phantom suggest that this avenue of research may be promising.

The second area of research concerns the model used to interpolate the deformation field in regions where there is no specific anatomical information available to establish correspondence. As described earlier, application of the ANIMAL algorithm results in deformation fields that can be used to approximate basis functions that truly represent anatomical variability. While these basis functions are dependent on method used to estimate the deformation fields, we propose a boot-strapping process to refine these functions in a hierarchical manner.

Other areas of research involve improving and extending different aspects of the current algorithm. For example, the recovery of the deformation is based on the assumption that there exists a one-to-one mapping between homologous points in different brains. Since neighbouring points within a particular brain structure of the source data set should be mapped to neighbouring points in the target, the non-linear deformation is constrained to be continuous throughout the domain of the brain. However, there exist neighbouring points in unconnected structures (such as on opposite sides of a sulcus, or on either side of the longitudinal fissure) that do not need to be mapped to neighbouring points in the target. Therefore, it may be desirable to allow discontinuities in the transformation at internal brain surfaces, e.g. surfaces that separate the cerebellum from the occipital lobe or that separate the temporal lobe from the inferior frontal lobe. While this may complicate the recovery of the global transformation, the definition of piece-wise continuous regions where the current ANIMAL algorithm can be applied is certainly possible. The main problem will then reside in the inversion of the discontinuous spatial deformation transformation required for segmentation. The problem may be posed as the warping of a set of independent domains (e.g., lobes, cerebellum, brain stem, etc.). As the morphological variability of these domains arises independently through ontology, this methodology may represent more meaningful biological information.

We have already applied the ANIMAL algorithm to the study of neuroanatomical morphometric variability [Collins et al., 1994b]. In this type of analysis, it will be important to be able to separate the estimated variability into that due to the algorithm and that truly due to anatomical variability. Gee et al. [1995] have developed a Bayesian framework for the regularization problem, and in so doing makes possible the analysis of the variance (or reliability) in the estimated mapping. We are looking into the feasibility of incorporating a similar construct here.

Finally, the target model used here is based on a single subject. Even though normal, the particular brain chosen may represent an extreme of normal variability. We have built an MRI atlas from 305 normal subjects [Evans et al., 1992a] in stereotaxic space that can be used to represent the most average brain and thus be used as a truly average standard target model. We are currently in the process of

constructing a probabilistic atlas of neuroanatomical structures where each voxel of the atlas represents the probability of finding a given structure at that voxel position within the standard model [Collins et al., 1994b].

In summary, the motivation for this work stems from the need to have a fully automatic procedure to identify and delineate meaningful anatomical regions of the human brain from volumetric MRI data. The automatic method presented herein goes beyond existing techniques in significant ways while retaining some of their best features. The reversal of the standard segmentation strategy, from matching geometric contours directly on image data, to one of registration followed by delineation has been shown to be valid. The structures identified by this method are comparable to those segmented manually and the experimental results on both simulated and real MRI data have shown that the method is accurate and robust.

NOTE ADDED IN PROOF

Since the paper was submitted, optimization of the algorithm has resulted in a fourfold increase in speed with regard to the times specified in the discussion and graphed in Figure 8. With these optimizations, the procedure requires less than 3 minutes at the first scale step (FWHM = 24mm) and only 10 minutes per iteration to have a vector estimated every 8mm in the volume. Application of the algorithm at full resolution (vectors estimated at every millimeter) requires approximately 10 hours for completion.

ACKNOWLEDGMENTS

The authors would like to express their appreciation for support from the Canadian Medical Research Council (SP-30), the McDonnell-Pew Cognitive Neuroscience Center Program, the U.S. Human Brain Project (HBP), NIMH and NIDA. This work forms part of a continuing project of the HBP-funded International Consortium for Brain Mapping (ICBM) to develop a probabilistic atlas of human neuroanatomy.

REFERENCES

Arata L, Dhawan AP, Broderick J, Gaskill M (1991): Model-based analysis of MR images of the brain. IEEE Eng Med Biol 13(3):1331–1332.

Arnold D, Riess G, Matthews P, Collins D, Francis G, Antel J (1992): Quantitation of disease load and progression in multiple sclerosis by means if proton magnetic resonance spectroscopy. In: Proceedings of the Society Magnetic Resonance in Medicine 11th Annual Meeting. Berlin: Society Magnetic Resonance in Medicine, p 1911.

Bajcsy R, Kovacic S (1989): Multiresolution elastic matching. Comput Vis Graphics Image Processing 46:1–21, 1989.

Bezdek JC, Hall LO, Clarke LP (1993): Review of MR image segmentation techniques using pattern recognition. Med Phys 20(4):1033–1048

Bohm C, Greitz T, Seitz R, Eriksson L (1991): Specification and selection of regions of interest (rois) in a computerized brain atlas. J Cereb Blood Flow Metab 11(2):A64–68.

Bohm C, Greitz T, Thurfjell L (1992): The role of anatomic information in quantifying functional neuroimaging data. J Neural Transm [Suppl] 37(37):67–78.

Bookstein FL (1989): Principal warps: Thin-plate splines and the decomposition of deformations. IEEE Trans Pattern Anal Machine Intelligence, PAMI-11(6):567–585.

Brodmann K (1909): Vergleichende Lokalisationlehre der Grosshirnrinde in ihren Prinzipien dargestellt auf Grund des Zellenbaues. Leipzig: J.A. Barth.

Broit C (1981): Optimal registration of deformed images. PhD thesis, University of Pennsylvania, Philadelphia, 1981.

Collignon A, Maes F, Delaere D, Vandermeulen D, Suetens P, Marchal G (1995): Automated multi-modality image registration based on information theory. In: Bizais Y, Barillot C, and Paola RD (eds): Information Processing in Medical Imaging (IPMI). Boston: Kluwer, pp. 263–274.

Collins DL (1994): 3-D model-based segmentation of individual brain structures from magnetic resonance imaging data. PhD thesis, McGill University, Montreal, Canada, December 1994.

Collins DL, Neelin P, Peters TM, Evans AC (1994a): Automatic 3D inter-subject registration of MR volumetric data in standardized talairach space. J Comput Assist Tomogr 18(2):192–205.

Collins DL, Peters TM, Evans AC (1994b): An automated 3D non-linear image deformation procedure for determination of gross morphometric variability in human brain. In: Proceedings of Conference on Visualization in Biomedical Computing. Rochester: SPIE 2359, pp 180–190.

Dhawan AP, Arata L (1992): Knowledge-based multi-modality three-dimensional image analysis of the brain. Am J Physiol Imaging 7(3–4):210–219.

Duchon J (1976): Interpolation des fonctions de deux variables suivant le principe de la flexion des plaques minces. R.A.I.R.O., Analyze numérique, 10:5–12.

Evans AC, Dai W, Collins DL, Neelin P, Marrett T (1991a): Warping of a computerized 3-D atlas to match brain image volumes for quantitative neuroanatomical and functional analysis. In Proceedings of the International Society of Optical Engineering: Medical Imaging V, volume 1445, San Jose, California, 27 February–1 March 1991. SPIE.

Evans AC, Marrett S, Torrescorzo J, Ku S, Collins L (1991b): MRI-PET correlation in three dimensions using a volume-of-interest (VOI) atlas. J Cereb Blood Flow Metab 11(2):A69–78.

Evans AC, Collins DL, Milner B (1992a): An MRI-based stereotactic atlas from 250 young normal subjects. Soc Neurosci Abstr 18:408.

Evans AC, Marrett S, Neelin P, Collins DL, Worsley K, Dai W, Milot S, Meyer E, Bub D (1992b): Anatomical mapping of functional activation in stereotactic coordinate space. NeuroImage 1(1): 43–53.

Evans AC, Collins DL, Mills SR, Brown ED, Kelly RL, Peters TM (1993): 3D statistical neuroanatomical models from 305 MRI volumes. In Proc. IEEE-Nuclear Science Symposium and Medical Imaging Conference, pp 1813–1817.

Evans AC, Kamber M, Collins DL, MacDonald D (1994): An MRI-based probabilistic atlas of neuroanatomy. In Shorvon S (ed): Magnetic Resonance Scanning and Epilepsy. New York: Plenum Press, pp 263–274.

Flechsig PE (1896): Gehirn und seele. Leipzig: Veit.

Fox PT, Perlmutter JS, Raichle ME (1985): A stereotactic method of anatomical localization for positron emission tomography. J Comput Assist Tomogr 9(1):141–153.

Gee J, LeBriquer L, Bariloot C (1995): Probabilistic matching of brain images. In Bizais Y, Barillot C (ed): Information Processing in Medical Imaging, France: Ile Berder.

Kall BA, Kelly PJ, Goerss AJ (1987): Comprehensive computer assisted data collection, treatment planning and interactive surgery. In Proceedings of SPIE Medical Imaging, volume 767. SPIE, pp 509–514.

Kamber M, Collins DL, Shinghal R, Francis GS, Evans AC (1992): Model-based 3D segmentation of multiple sclerosis lesions in dual-echo MRI data. In Proceedings of Conference on Visualization in Biomedical Computing, volume 1808. Chapel Hill, North Carolina, 13–16 October 1992. SPIE, pp 590–600.

Kamber M, Shinghal R, Collins D, Francis G, Evans A (1994): Model-based 3D segmentation of multiple sclerosis lesions from magnetic resonance brain images. IEEE Trans Med Imaging (accepted for publication).

Kelly P, Kall B, Goerss S (1983): Stereotactic CT scanning for the biopsy of intracranial lesions and functional neurosurgery. Appl Neurophysiol 46:193–199.

Koenderink J, van Doorn A (1987): Representation of local geometry in the visual system. Biol Cybern 55:367–375.

Lemoine D, Barillot C, Gibaud B, Pasqualini E (1991): A 3D C^1 stereotactic deformation model to merge multimodality images and atlas data. In Proceedings of Computer Assisted Radiology, pp 665–668.

MacDonald D, Avis D, Evans AC (1994): Multiple surface identification and matching in magnetic resonance images. In: Proceedings of Conference on Visualization in Biomedical Computing. Rochester: SPIE 2359, pp 160–169.

Nastar C, Ayache N (1993): Non-rigid motion analysis in medical images: A physically based approach. In Proceedings of Information Processing in Medical Imaging. Flagstaff, Arizona, pp 17–32.

Ono M, Kubik S, Abernathey C (1990): Atlas of Cerebral Sulci. Stuttgart: Georg Thieme Verlag

Peters TM, Henri CJ, Pike GB, Clark JA, Collins DL, Olivier A (1990): Integration of stereoscopic DSA with 3D image reconstruction for stereotactic planning. Stereotactic and Functional Neurosurgery 55:471–476

Pizer S, Culip T, Frederickson R (1990): Toward interactive object definition in 3D scalar images. In Höhne K, Fuchs H, Pizer S (eds): 3D Imaging in Medicine: Algorithms, Systems, Applications, Travemünde, Germany: NATO ASI Series, pp 83–106.

Schad LR, Boesecke R, Schlegel W, Hartmann GH, Sturm V, Strauss LG, Lorenz WJ (1987): Three dimensional image correlation of CT, MR, and PET studies in radiotherapy treatment planning of brain tumors. J Comput Assist Tomogr 11(6):948–954.

Schalenbrand G, Bailey P (1959): Introduction to Stereotaxis With an Atlas of the Human Brain. Stuttgart: G. Thieme.

Seitz R, Bohm C, Greitz T, Roland P, Eriksson L, Blomqvist B, Rosenqvist B, Nordell B (1990): Accuracy and precision of the computerized brain atlas programme for localization and quantification in PET. J Cereb Blood Flow Metab 10(4):443–457.

Sontag M, Cheng E, Reynolds R, Talton D, Wallace G, Waxler RE (1986): 3D graphics in radiation-therapy treatment planning. Med Phys 13(4):574–574.

Sorlie C, Collins D, Worsley K, Evans A (1995): Neuroanatomical variability: A quantitative study of young normal brains in stereotaxic space. Human Brain Mapping (in press).

Talairach J, Tournoux P (1988): Co-planar Stereotactic Atlas of the Human Brain: 3-Dimensional Proportional System: An approach to Cerebral Imaging. Stuttgart: Georg Thieme Verlag.

tar Haar Romeny B, Florack LM, Koenderink JJ, Viergever MA (1991): Scale space: Its natural operators and differential invariants. In Colchester ACF, Hawkes DJ (eds): Information Processing in Medical Imaging. Wye, UK: IPMI, p 239.

Terzopoulos D, Witkin A, Kass M (1988): Constraints on deformable models: recovering 3D shape and non-rigid motion. Artif Intell 36(1):91–123.

Vernazza G, Serpico SB, Dellepiane SG (1987): A knowledge-based system for biomedical image processing and recognition. IEEE Trans circuits systems CAS-34(11):1399–1416.

von Economo CF (1929): The Cytoarchitectonics of the Human Cerebral Cortex. Oxford Medical Publications. London: H. Milford.

Woods R, Mazziotta J, Cherry S (1993): MRI-PET registration with automated algorithm. J Comput Assist Tomogr 17:536–546.

Zachmann H (1991): Interpretation of cranial MR-images using a digital atlas of the human head. IEEE Trans Med Imaging 99–110.

Zhengping J, Mowforth PH (1991): Mapping between MR brain images and a voxel model. Med Inf (Lond), 16(2):183–193.